Coarse-Grained Molecular Simulations of Allosteric Cooperativity

Prithviraj Nandigrami and John J. Portman[1]
Department of Physics, Kent State University, Kent, OH 44242

(Dated: 15 March 2016)

Interactions between a protein and a ligand are often accompanied by a redistribution of the population of thermally accessible conformations. This dynamic response of the protein's functional energy landscape enables a protein to modulate binding affinities and control binding sensitivity to ligand concentration. In this paper, we investigate the structural origins of binding affinity and allosteric cooperativity of binding two Ca^{2+}ions to each domain of calmodulin (CaM) through simulations of a simple coarse-grained model. In this model, the protein's conformational transitions between open and closed conformational ensembles are simulated explicitly and ligand binding and unbinding is treated implicitly within the Grand Canonical Ensemble. Ligand binding is cooperative because the binding sites are coupled through a shift in the dominant conformational ensemble upon binding. The classic Monod-Wyman-Changeux model of allostery with appropriate binding free energy to the open and closed ensembles accurately describes the simulated binding thermodynamics. The simulations predict that the two domains of CaM have distinct binding affinity and cooperativity. In particular, C-terminal domain binds $Ca^{2+}$with higher affinity and greater cooperativity than the N-terminal domain. From a structural point of view, the affinity of an individual binding loop depends sensitively on the loop's structural compatibility with the ligand in the bound ensemble, as well as the conformational flexibility of the binding site in the unbound ensemble.

arXiv:1511.02268v2 [physics.bio-ph] 11 Mar 2016

INTRODUCTION

Conformational dynamics is essential for a protein's ability to exhibit allostery. The coupling between two distant binding sites is frequently accomplished by a conformational change between a "closed" (apo) to an "open" (holo) conformation upon ligation.[1] Although the end point conformations often give valuable insight into protein function, a detailed description of the allosteric mechanism for a particular protein requires one to consider a broader conformational ensemble. The landscape theory of binding[2–4] acknowledges that a folded protein is inherently dynamic and explores the thermally accessible conformational states in its native basin.[5] This conformational ensemble comprises the protein's "functional landscape".[6] While only a small subset of the states comprising the folding energy landscape[7], the functional landscape determines how a protein responds to the changes in its local environment such as ligand interactions. Due to the heterogeneous nature of the conformational ensemble, a ligand preferentially stabilizes some conformations more than others, causing the protein's thermal population to redistribute to a ligated ensemble which in general has distinct equilibrium properties.[8,9] The ensemble nature of allostery accommodates a rich and diverse set of regulatory strategies and provides a general framework to understand binding thermodynamics and kinetics of specific proteins.[10,11] Even simple landscapes with a small number of well defined basins separated by kinetic barriers can have subtle binding mechanisms because they depend on ligand interactions to short-lived transient states. Experimental progress on this challenging kinetics problem has appeared only very recently.[12] In principle, affinities of metastable states can also be obtained from thermodynamic binding measurements, although such analysis may not always be practical. In this paper, we focus on the cooperative binding of two Ca^{2+}ions to the binding loops of the domains of Calmodulin (CaM) through equilibrium coarse-grained simulations.

In this minimal model, the conformational transition between the open and closed ensembles are simulated explicitly and the dynamic shift in population due to ligand binding and unbinding is approximated by discrete jumps between a ligated and unligated free energy surfaces.[13] The protein dynamics are governed by a native-centric potential that couples the open and closed conformational basins while ligation is represented implicitly through ligand mediated protein contacts. This model, developed by Takada and co-workers, has been used to investigate the kinetic partitioning of induced fit and conformational selection binding pathways[14] as well as mechanical unfolding of Calmodulin in the presence of Ca^{2+}.[15] Here, we assume that the ligands bound to the protein are in equilibrium with a dilute solution and calculate binding thermodynamics as a function of ligand concentration.

The model is parameterized so that the closed basin is more stable than the open basin in the unligated ensemble. Ligands interact with all conformations in the ensemble, but the affinity is largest for conformations within the open basin due to their high structural compatibility with the ligand. Thus, the population shifts towards the open ensemble with increasing ligand concentration (see *SI* Fig.S1). The simulated ensembles have significant molecular fluctuations which modulate ligand affinities and affect the coupling between the binding sites. When binding thermodynamics are dominated by the open and closed ensembles, this model provides a molecular realization of the celebrated Monod-Wyman-Changeux (MWC) model of allostery.[16,17] For binding a single ligand the MWC model has four states: unligated-

open, unligated-closed, ligated-open, and ligated-closed. Appealing to this simple four-state model allows us to extract binding free energies of the isolated sites in the simulated open and closed ensembles and to calculate the free energy associated with the cooperative coupling between the sites. The simulations connect the conformational ensemble underlying the protein's dynamics with the MWC phenomenological binding parameters.[18]

Early work on binding thermodynamics of CaM has revealed that the affinities and cooperativities of the N-terminal domain (nCaM) and the C-terminal domain (cCaM) are distinct despite their structural similarity.[19–23] Although some experimental data has been reanalyzed recently[24–26], the traditional analysis of thermodynamic binding data has not used a dynamic landscape (or MWC) framework.[21,27,28] Nuclear Magnetic Resonance experiments[29–31] and all atom molecular dynamics simulations[32] that show a dynamic equilibrium between the open and closed conformations of CaM's domains in the absence of Ca^{2+}support our approach.

METHODS

Calmodulin (CaM) is a small, 148 amino acid long protein consisting of two topologically similar domains. Each domain consists of four α-helices and a pair of EF-hand Ca^{2+}-binding loops. The N-terminal domain (nCaM) has helices labeled A – D with binding loops I and II, and the C-terminal domain (cCaM) has helices labeled E – H with binding loops III and IV. We simulate open/closed allosteric transitions of the isolated domains of CaM using a native-centric model implemented in the *Cafemol* simulation package developed by Takada and co-workers.[13] This model couples two energy basins, one biased to the open (pdb: 1cll[33]) reference structure and the other biased to the closed (pdb: 1cfd[34]) reference structure. The energy of a conformation, specified by the N position vectors of the C-α atoms of the protein backbone, $\mathbf{R} = \{\mathbf{r}_1, \cdots \mathbf{r}_N\}$, is given by

$$V(\mathbf{R}) = \left(V_{\rm o}(\mathbf{R}) + V_{\rm c}(\mathbf{R}) + \Delta V\right)/2 - \sqrt{\left(V_{\rm o}(\mathbf{R}) - V_{\rm c}(\mathbf{R}) - \Delta V\right)^2/4 + \Delta^2}\,, \quad (1)$$

where $V_{\rm o}(\mathbf{R})$ is the single basin potential defined by the open structure and $V_{\rm c}(\mathbf{R})$ is the single basin potential defined by the closed structure. The interpolation parameters, Δ and ΔV, control the barrier height and the relative stability of the two basins. Parameters defining the single energy basins are set to their default values with uniform contact strength. The simulation temperature is set below the folding transition temperature of each of the four conformations. Specifically, the simulation temperature is set to $T_{\rm sim} = 0.8T_{\rm F}^{\star}$ where $T_{\rm F}^{\star} = 329$°K is the folding transition temperature corresponding to the closed (apo) state of nCaM, the lowest transition temperature among the open and closed states of nCaM and cCaM. Equilibrium trajectories of length 10^8 steps are simulated using Langevin dynamics with a friction coefficient of $\gamma = 0.25$ and a timestep of $\Delta t = 0.2$ (in coarse-grained units).[14]

Calcium binding to the two EF-hand loops of each domain of CaM is modeled implicitly by adding a potential defined from the ligand-mediated contacts in the EF-hand loops of the open (holo) conformation

$$V_{\rm bind} = -\sum_{i,j} c_{\rm lig}\epsilon_{\rm go} \exp\left[-\frac{\left(r_{ij} - r_{ij}^0\right)^2}{2\sigma_{ij}^2}\right]. \quad (2)$$

Here, the sum is over pairs of residues that are each within 4.5 $\mathring{A}$ of a Ca^{2+}ion and closer than 10.0 $\mathring{A}$ in the open (holo) conformation. The binding energy parameters $c_{\rm lig}$, $\epsilon_{\rm go}$, and σ are taken to be the same for each ligand-mediated contact for simplicity.

Binding cooperativity is influenced by the relative stability of the unligated open and closed states determined by ΔV and the binding free energy determined by $V_{\rm bind}$. In principle, these parameters can be adjusted to match measured binding properties. In the absence of clear measured constraints, we choose parameters so that the relative stability between the open and closed states are the same for each domain.

The transition barrier height is determined by Δ which is set to 14.0 kcal/mol for nCaM and 17.5 kcal/mol for cCaM. Adjusting $\Delta V = 5.0$ kcal/mol for nCaM and $\Delta V = 4.75$ kcal/mol for cCaM while keeping other parameters fixed gives an energy difference between the unligated open and closed states, $\epsilon = 4\,k_{\rm B}T$ for both domains. Experimentally, the folding temperatures of the N-terminal and C-terminal domains in intact CaM are approximately 328°K and 315°K, respectively.[35] Connecting to the domain opening kinetics in the intact protein, our simulation temperature corresponds to approximately 310°K which is 95% of nCaM's simulated folding temperature, and 98% of cCaM's simulated folding temperature. For the results reported in this paper, the binding energy parameters are set to $\epsilon_{\rm go} = 0.3$ (default value in *Cafemol*), $c_{\rm lig} = 2.5$ and $\sigma_{ij} = (0.1)r_{ij}^0$ where r_{ij}^0 is the corresponding separation distance in the open (holo) reference conformation. We have performed additional simulations to explore the dependence of binding thermodynamics on the ligand-mediated contact strength and interaction range. At higher values of $c_{\rm lig}$ and σ_{ij}, the affinities of ligand binding to individual loops increase. Nevertheless, the slope of the titration curve at the midpoint of the transition (a measure of binding cooperativity) remains the same (*SI* Fig.S2).

The simulated conformational ensembles are characterized structurally in terms of local and global order parameters based on the contacts formed in each sampled conformation. The set of native contacts in the open and closed conformations are separated into three groups: those that occur exclusively in either the open or the closed native structures, and those that are common to both states. A native contact in a given conformation is considered to be formed provided the distance between

the two residues is closer than 1.2 times the corresponding distance in the native conformation. Local order parameters $q_{\rm open}(i)$ and $q_{\rm closed}(i)$ are defined as the fraction of native contacts involving the i^{th} residue that occur exclusively in the open and closed native structures, respectively. Overall native similarity is monitored by corresponding global order parameters, $Q_{\rm open} = \langle q_{\rm open}(i)\rangle$ and $Q_{\rm closed} = \langle q_{\rm closed}(i)\rangle$, where the average is taken over the residues of the protein. We identify metastable conformational basins from minima in the free energy computed through the population histogram parameterized by $Q_{\rm open}$ and $Q_{\rm closed}$.

Ligand binding/unbinding events coupled with a conformational change of the protein is modeled within the Grand Canonical Ensemble. Throughout the protein's conformational transitions, the ligation state of each loop is determined stochastically through a Monte Carlo step attempted every 1000 steps in the Langevin trajectory. If the loop is unligated, a ligand is introduced to the binding loop ($V \to V + V_{\rm bind}$) with probability

$$P_{0\to 1} = \min[1, \exp\left[-(V_{\rm bind} - \mu)/k_{\rm B}T\right]]. \qquad (3)$$

If the loop is ligated, the ligand dissociates from the binding loop ($V + V_{\rm bind} \to V$) with probability

$$P_{1\to 0} = \min[1, \exp\left[(V_{\rm bind} - \mu)/k_{\rm B}T\right]]. \qquad (4)$$

Here, μ is the chemical potential of a bound ligand. At equilibrium, μ equals the chemical potential of the ligand in solution,

$$\mu = k_{\rm B}T \ln\left(\frac{c}{c_0}\right) + \mu_0\,, \qquad (5)$$

where c is the ligand concentration, and c_0 and μ_0 are the reference concentration and reference chemical potential, respectively. To compute binding curves, a series of simulations are preformed, each at a different value of the ligand chemical potential. These simulated titration curves are reported as function of the chemical potential, or equivalently, in terms of the relative ligand concentration defined through $\mu/k_{\rm B}T = \ln(c/\bar{c}_0)$ where $\bar{c}_0 = c_0 \exp(-\mu_0/k_{\rm B}T)$.

This approach with Monte Carlo acceptance rates given in Eq. 3 and Eq. 4 is oriented towards binding thermodynamics from the outset. Takada and co-workers present a different choice motivated by ligand binding kinetics.[14] Instead of introducing a chemical potential, ligand concentration enters their model through a variable binding attempt rate, while the attempt rate of unbinding is fixed. Binding titration curves can also be calculated in this model, but as a function of the binding attempt rate rather than the concentration directly.[15]

BINDING A SINGLE LIGAND

We first consider Ca^{2+}binding exclusively to each individual loop by simulating the conformational change of the entire domain while permitting binding only to a single site. As shown in Fig.1 (A) and Fig.1 (B), the bound population as a function of ligand concentration, $p_{\rm b}(c)$, follows a typical sigmoidal profile connecting a fully unbound population at low concentration and a fully bound population at high concentration. The overall binding strength of the individual loops is reflected in the dissociation constant, $K_{\rm d}$, shown in Table.I. Binding affinities of nCaM's loops are nearly the same, whereas the affinities of cCaM's loops are significantly different, with $\mathrm{K}_{\rm d}^{\rm (IV)} \approx 7\,\mathrm{K}_{\rm d}^{\rm (III)}$. Comparing the binding strength of CaM's loops, our simulations predict that $\mathrm{K}_{\rm d}^{\rm (III)} < \mathrm{K}_{\rm d}^{\rm (I)} \approx \mathrm{K}_{\rm d}^{\rm (II)} < \mathrm{K}_{\rm d}^{\rm (IV)}$.

TABLE I. Number of ligand-mediated contacts, dissociation constants, and binding free energies for the loops of CaM.

	$N_{\rm con}$	$K_{\rm d}/\bar{c}_0$	$\epsilon_{\rm c}$ [a]	$\epsilon_{\rm o}$ [a]
loop I	5	0.054	-1.3	-3.1
loop II	5	0.062	-1.3	-2.9
loop III	8	0.018	-1.3	-4.1
loop IV	5	0.13	-0.5	-3.0

[a] in kcal/mol

It is reasonable to expect that binding affinities from a uniform native-centric model correlate with the number of ligand mediated contacts, $N_{\rm con}$. While loop III does indeed have the most contacts and the greatest binding affinity, accounting for reduced affinity of loop IV compared to the loops of nCaM, each with the same number of contacts, requires more careful explanation. Such subtlety is not surprising because binding strength is sensitive to a protein's conformational flexibility that modulates ligand interactions in both the open and closed ensembles. The MWC model provides insight into the affinities for the individual binding loops. Using notations in Ref.36, the bound population in the MWC model can be expressed as

$$p_{\rm b}(\mu) = \left(e^{-\beta(\epsilon_{\rm c}-\mu)} + e^{-\beta(\epsilon+\epsilon_{\rm o}-\mu)}\right)/Z_1 \qquad (6)$$

where

$$Z_1 = 1 + e^{-\beta(\epsilon_{\rm c}-\mu)} + e^{-\beta\epsilon}\left(1 + e^{-\beta(\epsilon_{\rm o}-\mu)}\right) \qquad (7)$$

is the single ligand partition function. Here, $\epsilon_{\rm c}$ and $\epsilon_{\rm o}$ denote the binding free energies of the ligand to the closed and open ensemble, ϵ is the difference in stability between the unbound closed and open ensemble, and μ is the ligand chemical potential.

The coupling parameters of the Hamiltonian fix $\epsilon = 4k_{\rm B}T$ in the simulation, leaving the binding parameters, $\epsilon_{\rm c}$ and $\epsilon_{\rm o}$, to be determined from the simulated titration curves. These two parameters are under-determined by a fit to the bound state probability alone. The population of the open ensemble (regardless of ligation state) provides an additional constraint for parameters in the

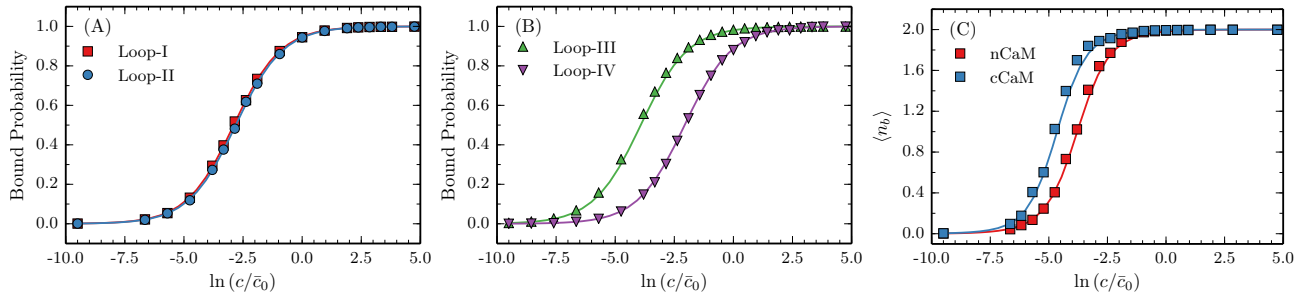

FIG. 1. Simulated binding curves for the individual loops of (A) nCaM and (B) cCaM. Lines are fits to the two state MWC model given by Eq.6. (C) Simulated mean number of bound ligands occupancy of binding sites with two ligands for nCaM (blue) and cCaM (red) as a function of ligand concentration. The solid lines plot $\langle n_{\rm b}(\mu)\rangle = p_{\rm b}^{\rm A0}(\mu) + p_{\rm b}^{\rm 0B}(\mu) + 2p_{\rm b}^{\rm AB}(\mu)$ with probabilities given from the MWC model evaluated with the binding parameters found from fits of binding to each individual loops.

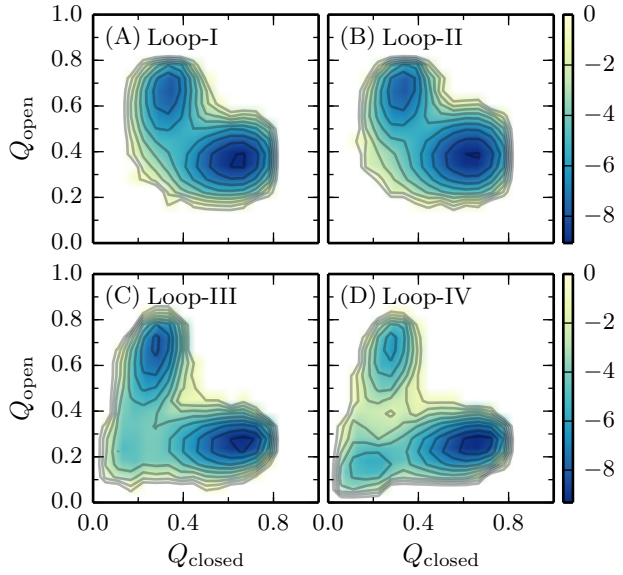

FIG. 2. Simulated free energy as a function of $Q_{\rm closed}$ and $Q_{\rm open}$ for binding loops at ligand concentration c = $K_{\rm d}$ for nCaM (A,B) and cCaM (C,D). The open state ensemble are conformations with $0.18 \leq Q_{\rm closed} \leq 0.35$ and $0.55 \leq Q_{\rm open} \leq 0.75$.

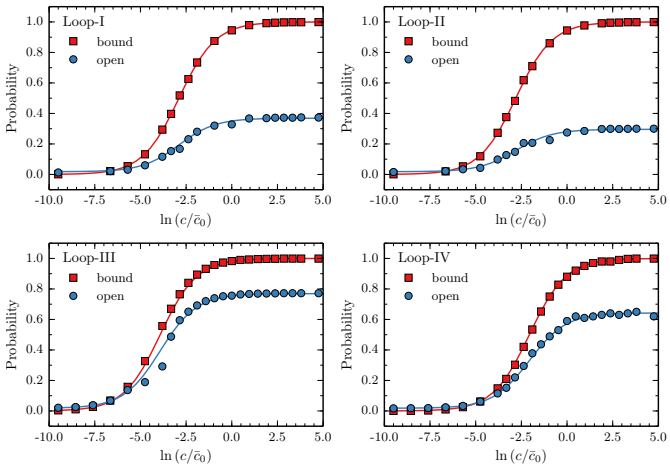

FIG. 3. Simultaneous fits of simulation data for a single ligand to $p_{\rm b}(\mu)$ and $p_{\rm o}(\mu)$ for individual binding loops. Solid curves are plots of $p_{\rm b}(\mu)$ and $p_{\rm o}(\mu)$ with $\epsilon_{\rm c}$ and $\epsilon_{\rm o}$ determined by a simultaneous fit to the simulation data (shown as points).

model. The open state configurations are identified in the simulations by global order parameters that measure the similarity to the open and closed native structures (see Fig.2). At high ligand concentration, the bound population saturates to unity. Since ligands bind to both the open and closed conformations, the limiting value of the open population, $p_o(\mu)$, is the fraction of ligated protein in an open conformation. As shown in Fig.3, the simulated open population of each loop saturates to a different limiting value determined by the relative stability of binding to the open and closed ensembles.

In the MWC model, the open state population

$$p_{\rm o}(\mu) = e^{-\beta\epsilon}\left(1 + e^{-\beta(\epsilon_{\rm o}-\mu)}\right)/Z_1 \qquad (8)$$

has a limiting value, $p_o(\beta\mu \gg 1) \sim [1 + e^{\beta(\epsilon+\Delta\epsilon)}]^{-1}$, that depends on $\Delta\epsilon = \epsilon_o - \epsilon_c$. Thus, $p_{\rm o}(\mu)$ and $p_{\rm b}(\mu)$ are independent constraints that can be used to determine reliable model parameters for the open and closed binding free energies, $\epsilon_{\rm o}$ and $\epsilon_{\rm c}$.

The binding free energies determined by a simultaneous fit to Eq.6 and Eq.8 are shown in Table.I. As expected, the dissociation constants depend on both $\epsilon_{\rm c}$ and $\epsilon_{\rm o}$. The values of $\epsilon_{\rm o}$ tracks the number of ligand mediated contacts in each loop, with loop III being the most stable, while the other loops have similar stability. The values of $\epsilon_{\rm c}$ is more subtle. Although loop III has more contacts than loop I and loop II, they all have the same $\epsilon_{\rm c}$. Thus, the relatively high affinity of loop III can be

attributed to its greater stabilization upon binding to the open state. The relatively low affinity of loop IV, in contrast, is explained by the smaller binding stabilization to the closed state.

Although experiments suggest that CaM's binding loops have heterogeneous affinities, assigning a binding strength to each loop is challenging because techniques to distinguish site-specific binding tend to alter the stability of the open and closed states.[37] Early studies which isolate the binding properties of loops III and IV of cCaM through site-directed mutagenesis indicate that loop IV has a higher propensity of Ca^{2+}-binding than loop III .[38,39] A similar approach indicates the affinity of the nCaM's loops are comparable, with loop I reported to have only 1.5 times higher affinity than the affinity of loop II.[40] On the other hand, isolating the loops by grafting them to a scaffold suggests a different order, with loop I having the highest affinity and loop III binding Ca^{2+}more tightly than loop IV.[41] Validation of our simulation results would benefit from experimental clarification of the relative binding affinities of the loops of CaM.

The effective binding free energies represent average properties over an ensemble that may include a broader range of conformations than those near the open and closed state minima. As shown in Fig.2, the conformational ensemble for binding to nCaM's loops are two state while the binding to cCaM's loops includes contribution from a partially unfolded basin as well. The appearance of an unfolded intermediate in the domain opening transition of Ca^{2+}-free cCaM was first reported by Chen and Hummer.[42] Distinct ensembles for nCaM and cCaM are consistent with the simulated transition mechanisms of the domains in the absence of Ca^{2+}(submitted). Although the four-state description of MWC is an approximation (especially for cCaM), it's use is validated by the accurate description of the populations of different ligation states for simulations of two ligand binding discussed in the next section.

BINDING TWO LIGANDS

We turn now to simulations in which both binding sites are accessible to the ligands. The mean number of bound ligands as a function of concentration, shown in Fig.1 (C), indicates that the effective dissociation constant of nCaM, $K_{\rm d}({\rm nCaM})/\bar{c}_0 = 2.2\times10^{-2}$, is roughly three times larger than the dissociation constant of cCaM, $K_{\rm d}({\rm cCaM})/\bar{c}_0 = 8.8\times10^{-3}$. For both domains, the midpoint concentration for binding two ligands is smaller than the dissociation constants for the individual binding sites in the domain. The finding that cCaM has greater overall binding affinity than nCaM agrees qualitatively with experiments.[22,43] Additionally, the estimated value of $K_{\rm d}$(nCaM) is within the experimentally reported range of approximately 6 – 10 times $K_{\rm d}$(cCaM).[19–21]

Binding curves calculated within the MWC model are also shown in Fig.1 (C). Denoting the two binding sites in the domains as site A (loop I or loop III) and site B (loop II or loop IV), we calculate $\langle n_{\rm b}(\mu)\rangle = p_{\rm b}^{\rm A0}(\mu) + p_{\rm b}^{\rm 0B}(\mu) + 2p_{\rm b}^{\rm AB}(\mu)$ where

$$p_{\rm b}^{\rm A0}(\mu) = (e^{-\beta(\epsilon_{\rm c}^{\rm A}-\mu)} + e^{-\beta(\epsilon+\epsilon_{\rm o}^{\rm A}-\mu)})/Z_2 \quad (9)$$

$$p_{\rm b}^{\rm 0B}(\mu) = (e^{-\beta(\epsilon_{\rm c}^{\rm B}-\mu)} + e^{-\beta(\epsilon+\epsilon_{\rm o}^{\rm B}-\mu)})/Z_2 \quad (10)$$

$$p_{\rm b}^{\rm AB}(\mu) = (e^{-\beta(\epsilon_{\rm c}^{\rm A}+\epsilon_{\rm c}^{\rm B}-2\mu)} + e^{-\beta(\epsilon+\epsilon_{\rm o}^{\rm A}+\epsilon_{\rm o}^{\rm B}-2\mu)})/Z_2 \quad (11)$$

are the probabilities for the conformational ensemble with site A occupied and site B empty, site B occupied and site A empty, and both binding sites simultaneously occupied, respectively. Here, $Z_2 = Z_{\rm c} + e^{-\beta\epsilon}Z_{\rm o}$ denotes the two ligand partition function with

$$Z_i = 1 + e^{-\beta(\epsilon_i^{\rm A}-\mu)} + e^{-\beta(\epsilon_i^{\rm B}-\mu)}, \quad i = ({\rm o},{\rm c}). \quad (12)$$

where, for example, $\epsilon_{\rm c}^{\rm A}$ and $\epsilon_{\rm o}^{\rm A}$ denotes the binding free energies to loop A (described in the previous section). The agreement between the MWC model and simulated binding curves is excellent, indicating that the binding cooperativity of the simulations is well characterized by the MWC Model.

The MWC model also quantitatively captures the simulated populations of individual ligation states as shown in Fig.4. Starting at low concentration, the growth of the singly ligated and the fully ligated states are concomitant. The fully loaded protein becomes increasingly stable, thereby reducing the singly ligated populations after certain threshold. The probability of exclusive binding to either loop of nCaM is equal, attaining a maximum population of 15% each. In contrast, virtually all of binding of the first ligand in cCaM occurs in loop III, reaching a maximum population of 20%. The near complete suppression of Ca^{2+}ligation exclusively to loop IV is due to its small relative binding affinity.

BINDING COOPERATIVITY

In cooperative binding, enhanced recruitment of a second ligand suppresses the population of singly ligated proteins thereby sharpening the binding curve. Within the assumptions of the MWC model, the shape of the binding curve is determined by two mechanisms. First, the greater stabilization of the open conformation over the closed conformation upon binding makes even binding a single ligand more sensitive to changes in concentration. The second source of cooperativity is the allosteric coupling provided by the assertion that the binding sites are either both open or both closed depending on the conformational state of the entire protein.

Comparing the simulated binding curves to those produced from a model that neglects both of these cooperative assumptions gives a qualitative sense of the simulated binding cooperativity. We consider the binding probabilities calculated according to the partition function for induced fit binding to independent binding sites.

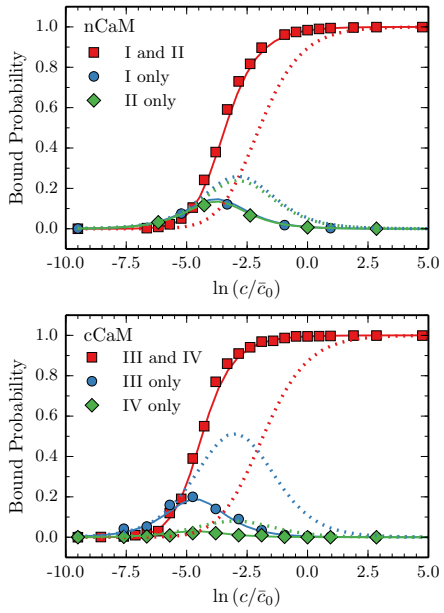

FIG. 4. Populations of ligation states $p_{\rm b}^{\rm A0}(\mu)$ (blue), $p_{\rm b}^{\rm 0B}(\mu)$ (green), and $p_{\rm b}^{\rm AB}(\mu)$ (red) plotted as a function of Ca^{2+}concentration for nCaM (top) and cCaM (bottom). Simulation data shown as points. Solid curves plot Eq.(9–11) from the MWC model. Dotted curves show plots of the non-cooperative induced fit model of binding to independent sites described by the partition function given in Eq.13. Note some data points are skipped for clarity.

These binding probabilities, shown in Fig.4, are calculated according to the partition function $Z_{\rm IF} = Z_{\rm A} Z_{\rm B}$ where

$$Z_\alpha = \left(1 + e^{-\beta(\epsilon_{\rm o}^\alpha - \mu)} + e^{-\beta(\epsilon_{\rm c}^\alpha - \mu)}\right), \quad \alpha = (A, B). \quad (13)$$

Compared to the simulations, the populations $p_{\rm b}^{\rm A0}(\mu)$ and $p_{\rm b}^{\rm 0B}(\mu)$ for independent binding to loops I – III initiate growth at smaller concentrations relative the the midpoint of $p_{\rm b}^{\rm AB}(\mu)$, and achieve a greater maximum. Exclusive binding to loop IV does not develop significant population even when the loops are independent. Comparing the two domains, the singly ligated states are suppressed more in cCaM's loop III than either of nCaM's loops. Furthermore, the binding curve sharpens more in cCaM than nCaM. These comparisons show that the simulated binding is indeed cooperative with cCaM having greater binding cooperativity than nCaM in qualitative agreement to experiments.[21,23]

The strength of the binding cooperativity for each domain can be determined quantitatively by considering the thermodynamic cycle shown in Fig.5. A Ca^{2+}ion can bind to either loop A or loop B of the unligated protein with equilibrium constant $K_{\rm A}$ and $K_{\rm B}$, respectively. The change in stability upon a Ca^{2+}ion binding to site B when site A is occupied, for example, can be expressed as $c_{\rm AB}K_{\rm B}$ where $c_{\rm AB}$ represents the additional stability associated with the presence of a previously bound

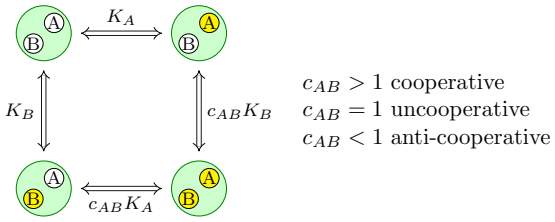

FIG. 5. Thermodynamic cycle for binding two ligands.

ligand to site A. A similar argument gives the equilibrium constant $c_{\rm AB}K_{\rm A}$ representing the change in stability when a Ca^{2+}ion binds to site A if site B is already occupied. The overall equilibrium constant of the fully ligated protein relative to the unligated protein is given by $K_2 = c_{\rm AB}K_{\rm A}K_{\rm B}$ which corresponds to the binding free energy, $\Delta F = -k_{\rm B}T \ln K_2$. The free energy associated with allosteric interactions between the ligands is therefore given by $\Delta F_{AB} = -k_{\rm B}T \ln c_{\rm AB}$.

In order to calculate $c_{\rm AB}$ for the simulated transitions, we express the equilibrium constants of the thermodynamic cycle in terms of populations of ligation states

$$K_{\rm A} = p_{\rm b}^{\rm A0}(\mu)/[p_{\rm ub}(\mu)\, c], \quad K_{\rm B} = p_{\rm b}^{\rm 0B}(\mu)/[p_{\rm ub}(\mu)\, c] \quad (14)$$

and

$$c_{\rm AB}K_{\rm A}K_{\rm B} = p_{\rm b}^{\rm AB}(\mu)/[p_{\rm ub}(\mu)\, c^2], \quad (15)$$

where $p_{\rm ub}(\mu)$ denotes the unbound population and c stands for the ligand concentration. Solving for $c_{\rm AB}$ gives

$$c_{\rm AB} = \frac{p_{\rm b}^{\rm AB}(\mu) p_{\rm ub}(\mu)}{p_{\rm b}^{\rm A0}(\mu) p_{\rm b}^{\rm 0B}(\mu)} \quad (16)$$

in terms of the population of ligated states. The value of $c_{\rm AB} = \exp(-\beta \Delta F_{\rm AB})$ reflects the degree of cooperativity of the transition. When the sites are independent, $p_{\rm b}^{\rm AB}(\mu) = p_{\rm b}^{\rm A}(\mu) p_{\rm b}^{\rm B}(\mu)/p_{\rm ub}(\mu)$, so that $c_{\rm AB} = 1$ as expected for uncoupled sites.

TABLE II. Simulated microscopic and macroscopic equilibrium constants

	$K_{\rm A}$ [a]	$K_{\rm B}$ [a]	$c_{\rm AB}$	K_1 [a]	K_2 [b]
nCaM	15.2	14.1	6.8	29.1	1.5×10^3
cCaM	40.0	6.7	29.6	46.7	8.0×10^3

[a] in units of $\bar{c}_0^{-1}$
[b] in units of $\bar{c}_0^{-2}$

Although the right hand side of Eq.16 can be evaluated directly from simulated populations, it is convenient to take advantage of the parameterization provided by the MWC model since it accurately describes the simulated equilibrium populations. Using Eq.(9–11) with $p_{\rm ub}(\mu) = (1 + e^{-\beta\epsilon})/Z_2$ leads to

$$c_{\rm AB} = \frac{[1 + \exp(-\beta\epsilon)]\,[1 + \exp(-\beta(\epsilon + \Delta\epsilon^{\rm A} + \Delta\epsilon^{\rm B}))]}{[1 + \exp(-\beta(\epsilon + \Delta\epsilon^{\rm A}))]\,[1 + \exp(-\beta(\epsilon + \Delta\epsilon^{\rm B}))]}, \quad (17)$$

with $\Delta\epsilon^{\rm A} = \epsilon_{\rm o}^{\rm A} - \epsilon_{\rm c}^{\rm A}$ and $\Delta\epsilon^{\rm B} = \epsilon_{\rm o}^{\rm B} - \epsilon_{\rm c}^{\rm B}$. The computed equilibrium constants, shown in Table.II, indicate that Ca^{2+}-binding to cCaM (with $c_{\rm AB} \approx 29.6$) is more cooperative than Ca^{2+}-binding to nCaM (with $c_{\rm AB} \approx 6.8$) in qualitative agreement with experiment.[21,23] The cooperative free energy is estimated to be $\Delta F_{\rm AB} \approx -3.4\, k_{\rm B}T$ for cCaM and $\Delta F_{\rm AB} \approx -1.9\, k_{\rm B}T$ for nCaM. The cooperative free energy for cCaM is 1.8 times that of nCaM in agreement with the experimental measured range of relative free energies of 1.2 – 3 reported in Ref.21 and Ref.44.

Binding thermodynamics determined from experiments that can not distinguish between binding to individual sites are often reported through the macroscopic equilibrium constants $K_1 = K_A + K_B$ and $K_2 = c_{AB}K_AK_B$.[27,28,44,45] The macroscopic equilibrium constants describing the simulated binding thermodynamics are shown in Table.II. The value of K_1 for cCaM is greater than K_1 for nCaM by a factor of 1.5 in agreement with the experimentally reported range of 1.2 – 2.2.[21,44] The free energy of binding two Ca^{2+}ions can be estimated from the macroscopic binding constants summarized in Table.II, $\Delta G_{\rm tot} = -k_{\rm B}T \log(K_1K_2)$. The simulated relative values of $\Delta G_{\rm tot}$ for cCaM is approximately 1.5 times the value of $\Delta G_{\rm tot}$ for nCaM, which is in agreement with experimentally reported value of approximately 1.1 – 1.3.[21,46] Taken together, the simulated values of the macroscopic binding constants for CaM are in qualitative agreement with those reported from experiments.

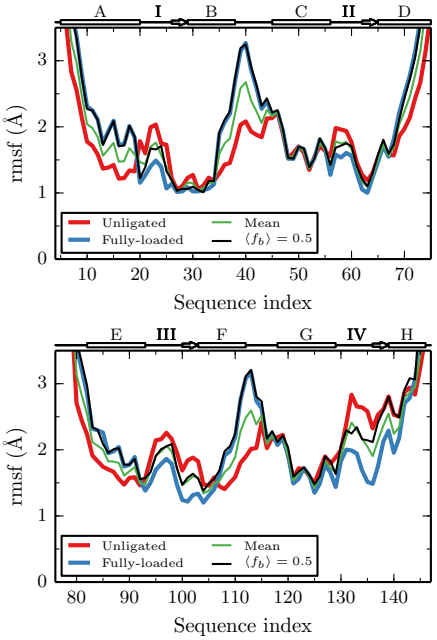

FIG. 6. Simulated root mean square fluctuations (rmsf) for each residue for nCaM (top) and cCaM (bottom) calculated at different ligand concentrations: high ligand concentration gives the fully saturated ensemble (blue curve), low ligand concentration gives the unligated ensemble (red curve), and at $K_{\rm d}$ (black curve). The rmsf curves are calculated for each ensemble after aligning to the open native conformation. (Aligning to the closed conformation give similar curves.) Also shown is the reference fluctuations given in Eq.18 (green curve).

MOLECULAR DESCRIPTION OF LIGAND BINDING

The simulations offer a detailed molecular description of Ca^{2+}binding as well as insight into the conformational ensembles underlying the binding free energies, $\epsilon_{\rm c}$ and $\epsilon_{\rm o}$. Fig.6 shows the root mean square fluctuations (rmsf) of each residue for the unligated (closed) ensemble at low ligand concentration and the fully saturated (open) ensemble at high ligand concentration. Focusing on nCaM, we see that helix A, the N-terminal end of helix B, and the B-C linker become more flexible upon Ca^{2+}-binding, while helix C and helix D show little change in flexibility. The temperature factors of the corresponding regions in cCaM show qualitatively similar behavior.

All four binding loops, on the other hand, become more rigid upon Ca^{2+}coordination. The difference in flexibility upon binding is largest for loop IV due to its large fluctuations in the unligated ensemble. Greater entropic stabilization of loop IV in the unligated state explains its relatively small binding affinity.[37] Furthermore, accounting for differences in loop entropy completes the rationalization of the binding free energies to the loops of CaM: while the value of $\epsilon_{\rm o}$ is dominated by the energetic stabilization of binding to the open state, the value of $\epsilon_{\rm c}$ reflects the degree of conformational entropy of the loop in the unligated ensemble.

The flexibility of individual residues are local order parameters that characterizes residue-specific conformational changes upon Ca^{2+}binding.[47] To qualitatively understand CaM's structural changes along the binding curve, we compare the fluctuations of the $i^{\rm th}$ residue to a two state reference rmsf, $\beta_0(i)$, given by average

$$\beta_0(i) = \langle f_{\rm b}\rangle\beta_{\rm o}(i) + (1 - \langle f_{\rm b}\rangle)\beta_{\rm c}(i), \qquad (18)$$

where the rmsf of the open ensemble, $\beta_{\rm o}(i)$, and the closed ensemble, $\beta_{\rm c}(i)$, are weighted by the fractional occupancy of the binding sites $\langle f_{\rm b}\rangle = \langle n_{\rm b}\rangle/2$. The structural ordering of a residue at any concentration can be characterized as early or late compared to mean flexibility $\beta_0(i)$ evaluated at the corresponding value of $\langle f_{\rm b}\rangle$. For example, Fig.6 shows the simulated rmsf of each residue at $K_{\rm d}$, as well as the reference fluctuations evaluated at $\langle f_{\rm b}\rangle = 1/2$. Although the Ca^{2+}occupancy of the binding loops is only 50%, the local environment of helix A and the B-C linker of nCaM as well as corresponding helix E and F-G linker of cCaM is already similar to that of the open state ensemble. This "early" transition to the open ensemble is a reflection of the allosteric cooperativity. In contrast, the average structural order of the binding loops is similar to the weighted average of the open and closed state flexibility. The exception is the β-sheet in the C-

terminal end of loop IV which takes on the open state structure at higher ligand concentrations. This "late" transition is in harmony with its lower binding affinity.

CONCLUDING REMARKS

In this paper, we introduce a method to simulate binding curves involving a protein that undergoes a conformational change upon binding. This approach allows us to identify the structural origins of binding affinity and to quantify allosteric cooperativity within a simple coarse-grained description of the protein dynamics. In this implicit ligand model, the protein conformation modulates the protein-ligand interactions through effective ligand-mediated contacts among residues in the binding site. The influence of ligand concentration on the effective binding strength is described through its uniform chemical potential.

Applying this approach to CaM, we find that this model can distinguish the binding properties of the two domains of CaM: binding loops I and II of nCaM have similar affinities, while in cCaM, binding loop III has significantly greater affinity than loop IV. The broader range of binding affinities in cCaM accounts for its greater cooperativity. Simulated populations of the ligation states as a function of concentration are accurately described by the MWC model with appropriate binding free energies for the individual loops. These binding free energies are average properties of the simulated ensemble and are not obvious solely from the open and closed structures. While the simulated binding thermodynamics is well-described by the MWC model, this simple analysis can obscure complexities in the free energy landscape. In separate publication, we describe how subtle differences in the topology and stability of the two domains lead to distinct simulated mechanisms for Ca^{2+}-free domain opening for nCaM and cCaM (submitted). In particular, we find that cCaM unfolds more readily than nCaM during the domain opening transition under similar conditions, a result consistent with the lower thermal stability of the C-terminal domain in the intact protein.[23,35] Although the unfolded conformations play a minor role in the binding thermodynamics described in this paper (aside from modifying the binding free energies to the open and closed states), global folding and unfolding in the domain opening transition likely has a significant qualitative influence on the binding kinetics. This is a problem we plan to address in future work.

ACKNOWLEDGMENTS

We would like to thank Daniel Gavazzi for help in figure preparation. Financial support from the National Science Foundation Grant No. MCB-0951039 is gratefully acknowledged.

[1] C. S. Goh, D. Milburn, and M. Gerstein, Curr. Opin. Struct. Biol. **14**, 104 (2004).
[2] B. Ma, S. Kumar, C. J. Tsai, and R. Nussinov, Protein Eng. **12**, 713 (1999).
[3] J. F. Swain and L. M. Gierasch, Current Opinion in Structural Biology **16**, 102 (2006).
[4] D. D. Boehr, R. Nussinov, and P. E. Wright, Nat. Chem. Biol. **5**, 789 (2009).
[5] K. Henzler-Wildman and D. Kern, Nature **450**, 964 (2007).
[6] P. I. Zhuravlev and G. A. Papoian, Quarterly Reviews of Biophysics **43**, 295 (2010).
[7] J. D. Bryngelson, J. N. Onuchic, N. D. Socci, and P. G. Wolynes, Proteins **21**, 167 (1995).
[8] S. Kumar, B. Ma, C. J. Tsai, N. Sinha, and R. Nussinov, Protein Sci. **9**, 10 (2000).
[9] R. G. Smock and L. M. Gierasch, Science **324**, 198 (2009).
[10] V. J. Hilser, J. O. Wrabl, and H. N. Motlagh, Annual Review of Biophysics **41**, 585 (2012).
[11] H. N. Motlagh, J. O. Wrabl, J. Li, and V. J. Hilser, Nature **508**, 331 (2014).
[12] K. G. Daniels, Y. Suo, and T. G. Oas, Proc. Natl. Acad. Sci. U. S. A. **112**, 9352 (2015).
[13] H. Kenzaki, N. Koga, N. Hori, R. Kanada, W. Li, K. Okazaki, X. Q. Yao, and S. Takada, Journal of Chemical Theory and Computation **7**, 1979 (2011).
[14] K. Okazaki and S. Takada, Proc. Natl. Acad. Sci. U. S. A. **105**, 11182 (2008).
[15] W. Li, W. Wang, and S. Takada, Proc. Natl. Acad. Sci. U. S. A. **111**, 10550 (2014).
[16] J. Monod, J. Wyman, and J. P. Changeux, J. Mol. Biol. **12**, 88 (1965).
[17] J. P. Changeux, Annual Review of Biophysics **41**, 103 (2012).
[18] Q. Cui and M. Karplus, Protein Sci. **17**, 1295 (2008).
[19] R. E. Klevit, Rachel E, D. C. Dalgarno, B. A. Levine, and R. J. Williams, European Journal of Biochemistry **139**, 109 (1984).
[20] C. L. A. Wang, Biochemical and Biophysical Research Communications **130**, 426 (1985).
[21] S. Linse, A. Helmersson, and S. Forsen, Journal of Biological Chemistry **266**, 8050 (1991).
[22] P. M. Bayley, W. A. Findlay, and S. R. Martin, Protein Sci. **5**, 1215 (1996).
[23] L. Masino, S. R. Martin, and P. M. Bayley, Protein Sci. **9**, 1519 (2000).
[24] M. I. Stefan, S. J. Edelstein, and N. Le Novère, Proc. Natl. Acad. Sci. U. S. A. **105**, 10768 (2008).
[25] M. I. Stefan, S. J. Edelstein, and N. Le Novère, BMC Systems Biology **3**, 68 (2009).
[26] M. Lai, D. Brun, S. J. Edelstein, and N. Le Novère, PLoS Comput. Biol. **11**, e1004063 (2015).
[27] B. R. Sorensen and M. A. Shea, Biochemistry **37**, 4244 (1998).
[28] R. A. Newman, W. S. Vanscyoc, B. R. Sorensen, O. R. Jaren, and M. A. Shea, Proteins: Structure, Function, and Bioinformatics **71**, 1792 (2008).
[29] G. Barbato, M. Ikura, L. E. Kay, R. W. Pastor, and A. Bax, Biochemistry **31**, 5269 (1992).
[30] J. Evenäs, S. Forsén, A. Malmendal, and M. Akke, J. Mol. Biol. **289**, 603 (1999).
[31] J. Evenäs, A. Malmendal, and M. Akke, Structure **9**, 185 (2001).
[32] D. Vigil, S. C. Gallagher, J. Trewhella, and A. E. García, Biophys. J. **80**, 2082 (2001).
[33] R. Chattopadhyaya, W. E. Meador, A. R. Means, and F. A. Quiocho, J. Mol. Biol. **228**, 1177 (1992).
[34] H. Kuboniwa, N. Tjandra, S. Grzesiek, H. Ren, C. B. Klee, and A. Bax, Nat. Struct. Biol. **2**, 768 (1995).
[35] C. R. Rabl, S. R. Martin, E. Neumann, and P. M. Bayley, Biophys. Chem. **101-102**, 553 (2002).
[36] S. Marzen, H. G. Garcia, and R. Phillips, J. Mol. Biol. **425**, 1433 (2013).
[37] J. Gifford, M. Walsh, and H. Vogel, Biochem. J. **405**, 199 (2007).
[38] J. Evenäs, A. Malmendal, E. Thulin, G. Carlström, and

S. Forsén, Biochemistry **37**, 13744 (1998).
[39]A. Malmendal, J. Evenäs, S. Forsén, and M. Akke, J. Mol. Biol. **293**, 883 (1999).
[40]M. R. Beccia, S. Sauge-Merle, D. Lemaire, N. Brémond, R. Pardoux, S. Blangy, P. Guilbaud, and C. Berthomieu, Journal of Biological Inorganic Chemistry **20**, 905 (2015).
[41]Y. Ye, H. W. Lee, W. Yang, S. Shealy, and J. J. Yang, J. Am. Chem. Soc. **127**, 3743 (2005).
[42]Y. G. Chen and G. Hummer, J. Am. Chem. Soc. **129**, 2414 (2007).
[43]J. Stigler and M. Rief, Proc. Natl. Acad. Sci. U. S. A. **109**, 17814 (2012).
[44]Y. Waltersson, S. Linse, P. Brodin, and T. Grundstroem, Biochemistry **32**, 7866 (1993).
[45]G. S. Adair *et al.*, Journal of Biological Chemistry **63**, 529 (1925).
[46]J. Jiang, Y. Zhou, J. Zou, Y. Chen, P. Patel, J. Yang, and E. Balog, Biochem. J. **432**, 89 (2010).
[47]S. Tripathi and J. J. Portman, Proc. Natl. Acad. Sci. U. S. A. **106**, 2104 (2009).

Supporting Information: Coarse-grained molecular simulations of allosteric cooperativity

ONE-DIMENSIONAL SIMULATED FREE ENERGY

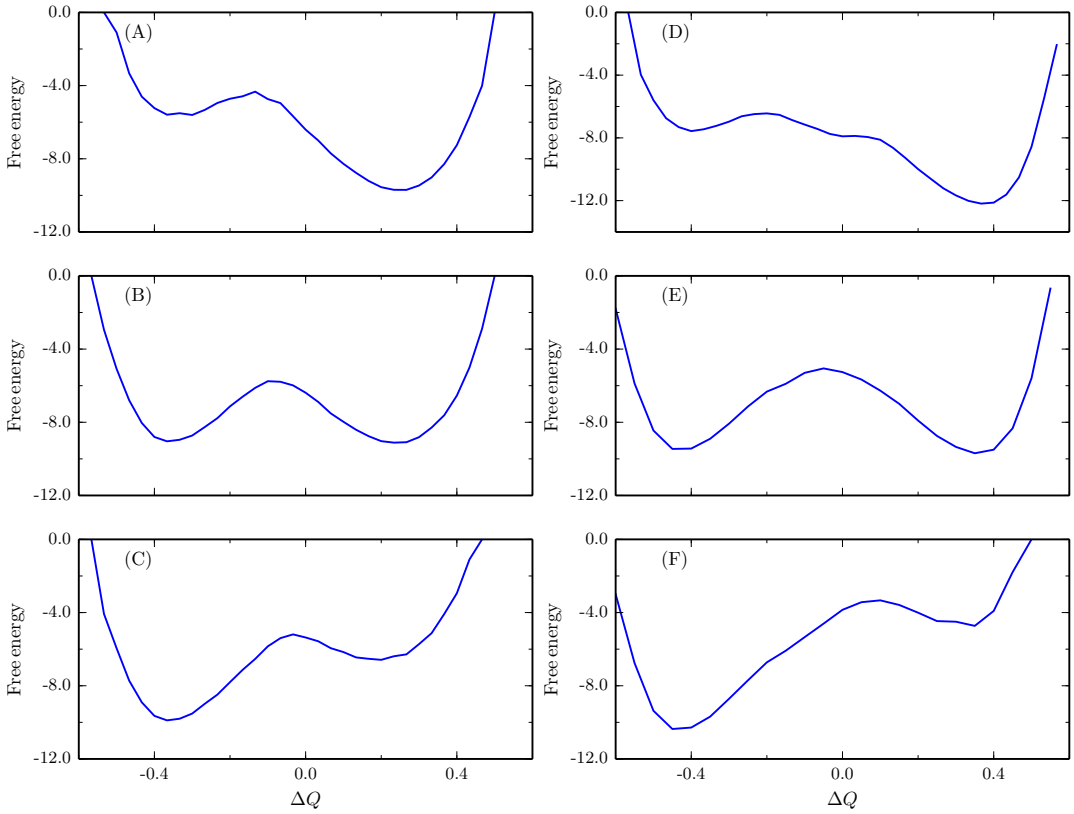

Figure S1. Simulated free energy for nCaM (A,B,C) and cCaM (D,E,F) corresponding to the ensemble of unligated (top), singly ligated (middle) and fully saturated (bottom) conformations. The x-axis represents simulated progress coordinate $\Delta Q = Q_{\text{closed}} - Q_{\text{open}}$ and the y-axis represents simulated free energy in units of $k_{\text{B}}T$.

Simulated free energy in terms of one-dimensional progress coordinate, $\Delta Q = Q_{\text{closed}} - Q_{\text{open}}$, as shown in Fig.S1, illustrates that for both domains, the closed state is more stable in the unligated ensemble. Binding of first ligand stabilizes both the closed and open states but the high affinity open state is stabilized to a greater extent due to its structural compatibility with the ligand. In the fully saturated ensemble, the open state has greater stability.

EXPLORING LIGAND CONTACT STRENGTH AND RANGE

For the results presented in the paper, we made specific choices for the ligand-mediated contact strength, $c_{lig} = 2.5$, and interaction range, $\sigma_{ij} = (0.1)r^0_{ij}$, respectively. As shown in Fig.S2, with the increase of c_{lig} and σ_{ij}, the value of K_d for individual loops decreases. However, the slope of the binding transition curve at a concentration for which $p_{bound} = 0.5$ remains the same. Here, we only show results for binding loop I as an illustration.

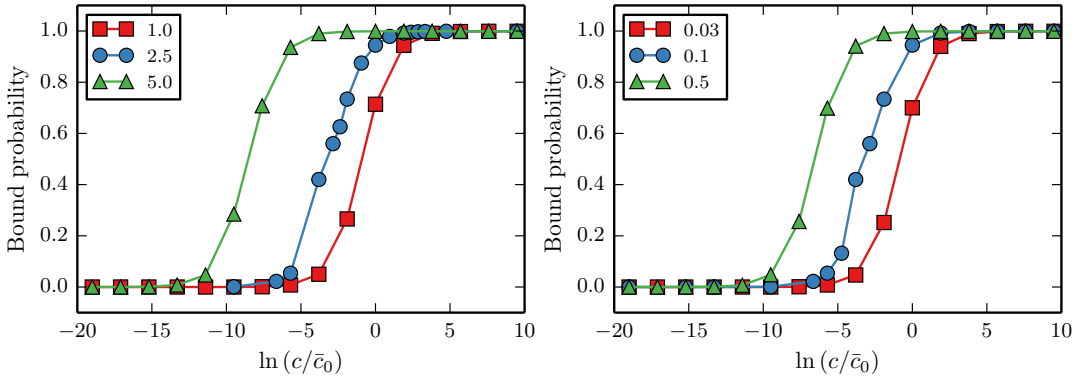

Figure S2. Simulated binding curves for loop I of nCaM with varying c_{lig} (left) and σ_{ij} (right). Consistent behavior is observed for other binding loops (data not shown).